ACS APPLIED MATERIALS & INTERFACES

Research Article

www.acsami.org

Revealing the Role of TiO_2 Surface Treatment of Hematite Nanorods Photoanodes for Solar Water Splitting

Xianglin Li,[†] Prince Saurabh Bassi,[‡] Pablo P. Boix,[†] Yanan Fang,[†] and Lydia Helena Wong*[,†,‡]

[†]Energy Research Institute @ NTU, Nanyang Technological University, 50 Nanyang Drive, Research Techno Plaza, X-Frontier Block, Level 5, Singapore 637553

[‡]School of Materials Science and Engineering, Nanyang Technological University, Singapore 639798

Supporting Information

ABSTRACT: Ultrathin TiO_2 is deposited on conventional hydrothermal grown hematite nanorod arrays by atomic layer deposition (ALD). Significant photoelectrochemical water oxidation performance improvement is observed when the ALD TiO_2-treated samples are annealed at 650 °C or higher temperatures. The electrochemical impedance spectroscopy (EIS) study shows a surface trap-mediated charge transfer process exists at the hematite−electrolyte interface. Thus, one possible reason for the improvement could be the increased surface states at the hematite surface, which leads to better charge separation, less electron−hole recombination, and hence, greater improvement of photocurrent. Our Raman study shows the increase in surface defects on the ALD TiO_2-coated hematite sample after being annealed at 650 °C or higher temperatures. A photocurrent of 1.9 mA cm^{-2} at 1.23 V (vs RHE) with a maximum of 2.5 mA cm^{-2} at 1.8 V (vs RHE) in 1 M NaOH under AM 1.5 simulated solar illumination is achieved in optimized deposition and annealing conditions.

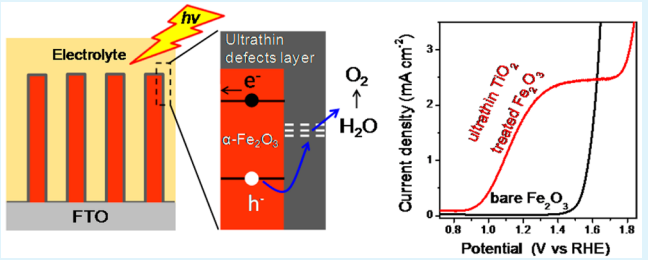

KEYWORDS: *photoelectrochemical cells (PEC), hematite, atomic layer deposition (ALD), nanorods, TiO_2, surface treatment*

1. INTRODUCTION

Photoelectrochemical cells (PEC) offer the ability to harness solar photons to split water, thereby producing hydrogen as a chemical fuel.[1−3] Hematite (α-Fe_2O_3) is a very promising material for PEC water splitting because of its favorable optical band gap (~2.1 eV), excellent stability under caustic operating conditions, earth abundance, and low cost.[4,5] The theoretical solar-to-hydrogen efficiency based on a semiconductor with this band gap can achieve a value of 16.8%.[6] However, the overall water splitting efficiency of hematite photoanodes falls well short of the theoretical maximum efficiency, primarily due to the very short electron−hole pair lifetime (<10 ps) and hole diffusion length (2−4 nm), which gives rise to a high recombination rate of photogenerated carriers in the bulk.[4] Considerable efforts have been devoted to improve the actual PEC performance of hematite by employing nanostructuring strategies,[7−15] as well as introducing dopant atoms into hematite.[16−25] In addition, the kinetics of the interfacial extraction of holes from the hematite surface for water oxidation (oxygen evolution) reaction seems to be sluggish, which results in increased charge recombination with a concomitant loss of photocurrent and hence the efficiency. In most of the reports, the surface traps have been suggested as an additional loss mechanism in various hematite photoanodes.[26−29] Indeed, improved hematite-based photochemical water splitting has been reported through passivating of surface states using very thin passivating layers, such as $Fe_xSn_{1-x}O_4$,[30] ALD Al_2O_3,[26] and ALD TiO_2.[26,31] However, a surface trap-mediated charge transfer process at the hematite-electrolyte interface has been suggested by Bisquert and their co-workers based on their electrochemical impedance spectroscopy (EIS) study, in which the water oxidation takes place predominantly from surface trapped holes, not directly from valence band holes.[32] In such a charge transfer mode, the surface states help the charge injection at the hematite and electrolyte interface. Thus, there could be a new surface treatment strategy to improve the photoelectrochemical water oxidation by increasing those surface states and consequently enhancing the charge transfer at the hematite/electrolyte interface.

In this work, we report a novel surface treatment strategy to improve the charge transfer of hematite photoanode by coating the hematite surface with an ultrathin TiO_2 layer using ALD and followed by an appropriate heat treatment at 650 °C. We perform a systematic investigation of the role of the treatments by accurately controlling the thickness and deposition conditions of the TiO_2 overlayer. During the annealing process, as the solid-state diffusion reaction occurs between the hematite and the TiO_2 overlayer, Ti is gradually incorporated into hematite from the surface. Simultaneously, small amount of Fe is diffused into the TiO_2 layer leading to the amorphization of TiO_2. The increased Raman intensity of the LO mode of

Received: February 12, 2015
Accepted: July 20, 2015
Published: July 20, 2015

DOI: 10.1021/acsami.5b01394
ACS Appl. Mater. Interfaces 2015, 7, 16960−16966

hematite shows the increase of surface defects at hematite surface after the solid reaction. EIS measurements show the presence of a trap-mediated charge transfer at the hematite-electrolyte, which can be shifted to higher potentials with the ALD TiO_2 layer. With optimized ALD TiO_2 thickness and post annealing time at 650 °C, a photocurrent of 1.9 mA cm^{-2} at 1.23 V (vs RHE) is achieved. This novel surface treatment strategy can be further applied to a broader range of nanostructured hematite photoanodes prepared by other methods

2. EXPERIMENTAL SECTION

2.1. Preparation of Hematite Nanorod Arrays and ALD TiO_2 Coating. Hematite nanorod arrays were grown on fluorine-doped tin oxide substrates (FTO, thickness 2.2 mm, resistance <14 ohm/square, transmittance >90%, purchased from Wuhan Geao, China) using a hydrothermal method. Typically, a 50 mL aqueous solution containing 10 mmol of $FeCl_3 \cdot 6H_2O$ (Sigma, ACS reagent 97%) and 15 mmol of urea (Sigma, 98%) was transferred into a 100 mL glass bottle and 12 substrates (1 cm × 2.5 cm) were placed vertically standing at the bottom of the bottle, then sealed with a cap. After 10 h of reaction at 100 °C, a uniform layer of yellow FeOOH film was formed on the FTO substrate. The substrates were thoroughly rinsed in distilled water (DI) water and blow-dried with N_2 gun. After annealing at 550 °C under air for 2 h, FeOOH was transformed to hematite. ALD TiO_2 was conducted on a Fiji 200 system with Tetrakis dimethylamino titanium (TDMATi) and H_2O as precursors at 120 °C. The TDMATi source was kept at 70 °C to achieve a suitable vapor pressure. The precursors were pulsed in the reactor with 40 sccm constant Ar flow, and the base pressure for deposition was 0.8 Torr. The pulse time for Ti and H_2O were 0.6 and 0.1 s, respectively. The purge time was 10 s for both precursors. The growth rate per cycle of TiO_2 was 0.06 nm, which is inconsistent with previous report.[33] After ALD TiO_2 coating, the hematite samples were kept horizontally inside a tube furnace in ambient condition and heated up to 650 °C with a heating rate of 25 °C/min, and kept at this temperature for different times (e.g., 30 min, 60 min, 90 min).

2.2. Characterization of Samples. Morphology of samples was characterized by a JEOL, JSM-7600F field emission scanning electron microscope (FESEM), high-resolution transmission electron microscopy (HRTEM) and scanning TEM (JEOL 2100F). The hematite nanorods were scraped from the FTO substrate and followed by a ultrasonic treatment in ethanol for TEM sample preparation. Raman spectra were collected on Renishaw inVia Raman system with 532 nm excitation wavelength, and a 50× objective lens was used in our measurement. Diffuse reflectance ultraviolet−visible (UV−vis) absorption spectra of the films were obtained using an Agilent Cary series UV−vis−NIR spectrophotometer (model Cary 500) equipped with an external diffuse reflectance accessory (DRA-2500). The diameter of integrating sphere is 150 mm. X-ray photoemission spectroscopy (XPS) was collected on a home-built ultra high vacuum (UHV) system with a monochromatic X-ray source at $h\nu$ = 1486.7 eV (Al, Kα) from SPECS and Omircon electron analyzer (EA125).

2.3. Photoelectrochemical Property Measurements. PEC measurements were carried out using CHI 660D workstation (CH Instruments, Inc.) with a three-electrode electrochemical system in 1 M NaOH (pH 13.6) electrolyte. Platinum mesh and Ag/AgCl were employed as counter and reference electrodes, respectively. The working surface area was 0.3 cm^2. The light source was simulated sunlight from a 150 W xenon solar simulator (67005, Newport Corp.) through a solar filter with a measured intensity equivalent to standard AM1.5 sunlight (100 mW cm^{-2}) on the sample surface. IPCE characteristics were measured with a xenon light source (MAX-302, Asahi Spectra Co. Ltd.) coupled with a monochromator (CMS-100, Asahi Spectra Co. Ltd.) from 305 to 630 nm, at a potential of 1.23 V vs RHE. A Si photodiode (Bentham, DH-Si) with known IPCE was used to calculate the IPCE of the pure hematite and TiO_2-treated hematite photoanodes. A source meter (Keithley Instruments Inc., Model: 2400) was used to measure the photocurrent of Si diode. The working station (CHI 660D, CH Instruments, Inc.) mentioned above was used to measure the photocurrent of samples. The EIS measurements were carried out using an Autolab PGSTAT 302F in a three-electrode electrochemical system. A sinusoidal voltage perturbation of 20 mV was applied from 100 kHz to 0.1 Hz, with a DC voltage sweep over the range of interest. The same reference and counter electrodes used for PEC measurements were used.

3. RESULTS AND DISCUSSION

Figure 1a, b shows the top-view and cross-section SEM images of the as grown hematite nanorod arrays coated with 40 cycles

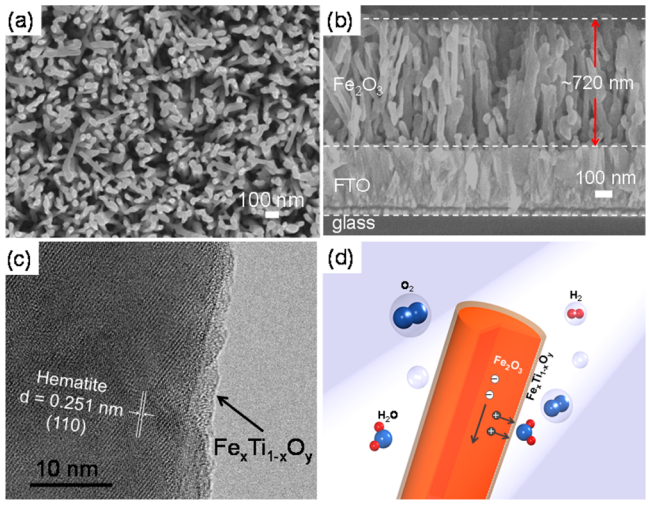

Figure 1. SEM image of the ALD TiO_2-coated hematite after being annealed at 650 °C for 30 min: (a) top view and (b) cross-section image. (c) HRTEM of 40 cycles of ALD TiO_2-coated hematite after annealed at 650 °C for 30 min. (d) Schematic effect of ultrathin ALD TiO_2 overlayer on hematite nanorods for efficient solar water splitting.

of ALD TiO_2 overlayer and annealed at 650 °C for 30 min. As the TiO_2 over layer is very thin, ~2.5 nm for 40 cycles, morphology remains similar to the pristine hematite nanorods arrays. The morphology of the hydrothermal FeOOH and the pristine hematite without ALD TiO_2 coating are shown in Figure S1. The diameter of the nanorods is around 60 to 80 nm, and the length is ~700 nm. The aspect ratio of the hematite nanorods is around 10. Figure 1c shows a typical HRTEM image of the hematite nanorod arrays sample with 40 ALD TiO_2 cycles and post annealed at 650 °C for 30 min. The lattice of the hematite core can be clearly seen. The amorphous overlayer around the hematite nanorod surface could also be observed. The thickness of the overlayer is around 2 nm, which is consistent with the estimated ALD TiO_2 thickness (2.4 nm for 40 ALD cycles). To further investigate the ultrathin amorphous overlayer, Raman, XRD, and STEM measurements were carried out. Figure 2 shows the Raman spectra of the TiO_2 coated hematite samples annealed at different temperatures (400 and 650 °C) and the pristine hematite nanorod arrays annealed at 650 °C for comparison. All the Raman peaks of the pristine sample: 224, 244, 291, 297, 410, 499, 610, and 660 cm^{-1} can be assigned to hematite.[34] After ALD TiO_2 and further annealing at 400 °C for 30 min, a small but obvious Raman peak at 143 cm^{-1} (red marked in Figure 2) assigned to anatase TiO_2 E_g mode is observed,[35] and all the Raman peaks assigned to hematite remained with no obvious change. This suggests that the nanorod structure consist of hematite core

DOI: 10.1021/acsami.5b01394
ACS Appl. Mater. Interfaces 2015, 7, 16960−16966

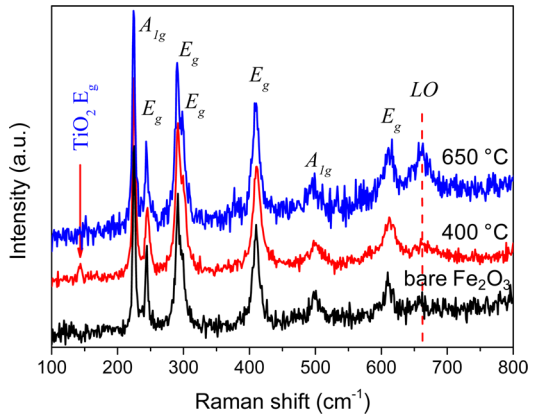

Figure 2. Raman spectra of the pristine hematite nanorod arrays (black curve), ALD TiO_2-coated hematite annealed at 400 °C (red curve), and 650 °C (blue curve), respectively.

and TiO_2 shell after the 400 °C annealing. By increasing the post annealing temperature to 650 °C, the Raman peak of TiO_2 at ∼143 cm^{-1} disappears and the intensity of the hematite LO mode peak (∼660 cm^{-1}) dramatically increases (Figure 2). It should be noted that the LO mode of hematite at 660 cm^{-1} is normally forbidden by the selection rules, so the origin of this band is attributed to the breakdown of Raman symmetry selection rules induced by short-range order or lattice defects, as in the case of nanodimensions due to a large amount of surface defects.[36−38] All these observations indicate occurrence of solid reaction between TiO_2 overlayer and hematite core when annealed at 650 °C. During the annealing process a small amount of Fe ions diffused into the TiO_2 layer leading to amorphization of TiO_2 layer. However, this cannot be observed by XRD due to the overlap of the XRD peaks of TiO_2 and SnO_2 (from FTO substrate, Figure S2). Simultaneously, some Ti atoms on the surface diffused into the hematite core,[14] which may increase the surface defects and lattice distortion of hematite. The XRD pattern of the hematite nanorods shows a preferential orientation of the (110) peak, as the hematite growth direction is along (110) direction, as seen the HRTEM image in Figure 1c. The absence of peak shift or broadening of hematite in Raman and XRD (Figure 2 and Figure S2) studies also implies that the modifications due to ALD TiO_2 treatment are limited to the surface of the hematite nanorods. STEM images and elemental mapping of the hematite nanorod also show a uniform distribution of Ti (see Figure S3).

XPS was used to verify the Ti incorporation of the ALD TiO_2 coated hematite nanorods arrays. Figure 3a shows the survey scan of the TiO_2 coated hematite after annealed at 650 °C together with the bare hematite. Both spectra shows the same features of the hematite in Fe 2p and the existence of O. But only the ALD TiO_2 coated sample shows the Ti signal. The binding energies of Ti $2p_{1/2}$ and $2p_{3/2}$ are observed at 464.5 and 458.3 eV, respectively, indicating a normal state of Ti^{4+}.[25] The Fe $2p_{3/2}$ peak of the ALD TiO_2 treated hematite sample slightly shift to the lower energy side compared to that for the bare hematite sample, as seen in Figure 3b. This is consistent with expected binding energy shift based on the fact that electronegativity of Ti (1.54) is lower than that of Fe (1.83). The substitution of Fe with Ti in O−Fe−O will thereby lower the binding energy. Figure S4 shows the O 1s peak of the bare Fe_2O_3 and the ALD TiO_2 treated Fe_2O_3. The O 1s peak for the bare Fe_2O_3 sample is centered around 529.9 eV, which is

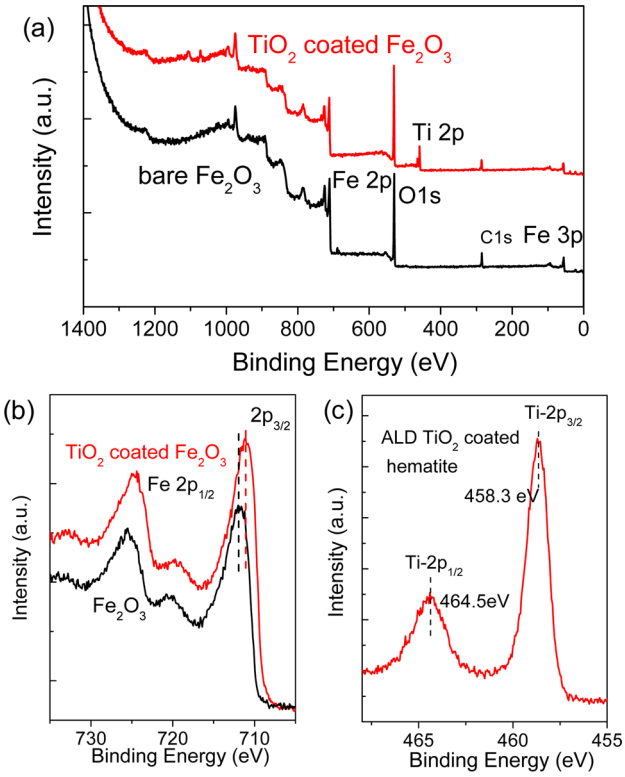

Figure 3. (a)XPS survey of the bare hematite nanorod arrays after being annealed at 650 °C and the ALD TiO_2 40 cycle coated hematite sample annealed at 650 °C. (b) Fe 2p details for the bare hematite and ALD TiO_2-coated hematite sample after being annealed at 650 °C. (c) Ti 2p chemical details for the ALD-coated hematite.

consistent with the reported value.[25] After ALD TiO_2 treatment the O 1s peak is shifted to slightly higher energy, which is consistent with pervious study of the Ti doped hematite.[25] From the XPS spectra, there is no Sn signal detected, which indicates the Sn diffusion from FTO substrate effect is minimum (and perhaps nonexistent) in our study. Diffused reflectance UV−vis spectra and corresponding Tauc-Plots of our samples are shown in Figure S5. The band gap obtained from Tauc-Plots for all the samples are almost the same, ∼2.05 eV. The slight change of band gap implies that Ti doping in the hematite nanorods is insignificant.

Figure 4 shows the photocurrent−potential (J−V) curves of the pristine hematite and hematite coated with 40 cycles ALD TiO_2 layers annealed at different temperatures. Negligible photocurrent is observed for the pristine hematite sample annealed at 650 °C, which is consistent with the previous report.[24] The photoresponse of the hematite coated with ALD TiO_2 and annealed at 400 °C is similar to the one of the pristine hematite. The only difference is the potential at which the current rise is shifted from ∼1.5 to ∼1.7 V vs RHE, similar to the observation of the dark current (Figure S6). This could be due to the formation of the heterojunction between hematite and TiO_2, as TiO_2 has much lower valence band,[39] which blocks the hole transfers and hence higher bias is needed for dark current onset. When the annealing temperature is increased to 650 °C, significant photocurrent can be observed. With this annealing temperature a solid reaction occurs between the hematite and TiO_2 over layer. When the annealing temperature is further increased to 750 °C only a little change in J−V curve is observed. Thus, the occurrence of the solid

DOI: 10.1021/acsami.5b01394
ACS Appl. Mater. Interfaces 2015, 7, 16960−16966

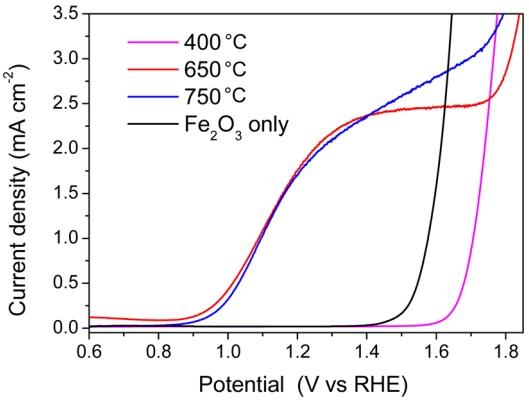

Figure 4. Photocurrent vs potential curves of 40 ALD TiO_2 cycle coated hematite photoanodes with different post-annealing temperatures.

reaction is more critical to the PEC improvement than the unintentional Sn doping from FTO, which usually occurs after annealed at 750 °C.[30]

To investigate into the role of the ALD TiO_2 surface treatment on the PEC performance, we systematically carried out a variation of TiO_2 thickness and annealing time. PEC was measured on hematite samples with different ALD TiO_2 thicknesses (from 20 to 160 cycles) and annealing times (30 to 90 min) at 650 °C, the results are shown in Figure 5. For 30 min annealing treatment at 650 °C, the photocurrent density improves when the ALD TiO_2 cycles are increased from 20 to 80. However, a further increase in the ALD TiO_2 cycles beyond 80 results in a reduction of the photocurrent density (see Figure 5a, c). The current density for the 80 cycles ALD TiO_2 coated sample reaches ~1.1 mA cm^{-2} at 1.23 V vs RHE in 1 M NaOH electrolyte (pH 13.6). A photocurrent onset potential of ~0.9 V vs RHE is observed for the samples with 20 ALD TiO_2 cycle numbers; while for the samples with thicker TiO_2 overlayers the onset potential shifted positively, reaching ~1.1 V vs RHE for the sample with 160 ALD cycles TiO_2 overlayer as shown in Figure 5a. The shifting of the onset potential with thicker ALD TiO_2 overlayer could be due to the formation of a heterojunction between Fe_2O_3 and TiO_2, which eventually inhibits the charge transport across the junction and limits the overall PEC performance. Figure 5b shows the annealing time effect with the ALD cycles fixed to 40 cycles. The photocurrent improves when the annealing time increases from 30 to 60 min, and then decreases slightly for 90 min annealing time. The increase of the photocurrent when the annealing process is prolonged to 60 min could be due to the further increase of the defects states as the solid state reaction at the Fe_2O_3/TiO_2 progresses, which will be discussed later. When the annealing time is longer than 60 min, the slight decrease in the photocurrent may be a result of the loss in the conductivity of FTO substrate.[40] Figure 5d shows the photocurrent densities under key potentials versus the annealing time. At the optimized ALD TiO_2 coating of 40 cycles (~2.4 nm) and annealing time of 60 min at 650 °C, the photocurrent at 1.23 V vs RHE is ~1.9 mA cm^{-2}, which is close to the highest reported photocurrent of 2.4 mA cm^{-2} at 1.23 V for hematite prepared by APCVD without using any catalyst,[12] and reaches a plateau of about 2.4 mA cm^{-2} at 1.4–1.7 V before the current increases exponentially, see Figure 5b. IPCE measurement shows the optimized sample can reach 25%, see Figure S7. The *I*–*T* curve in Figure S8 shows excellent stability of our hematite photoanode.

The electrical effects of the surface treatment with ALD TiO_2 and post annealing were studied by EIS. The pristine Fe_2O_3 and Fe_2O_3 coated with 40 ALD TiO_2 (post annealed at 650 °C for 1 h) samples were analyzed under illumination with a DC

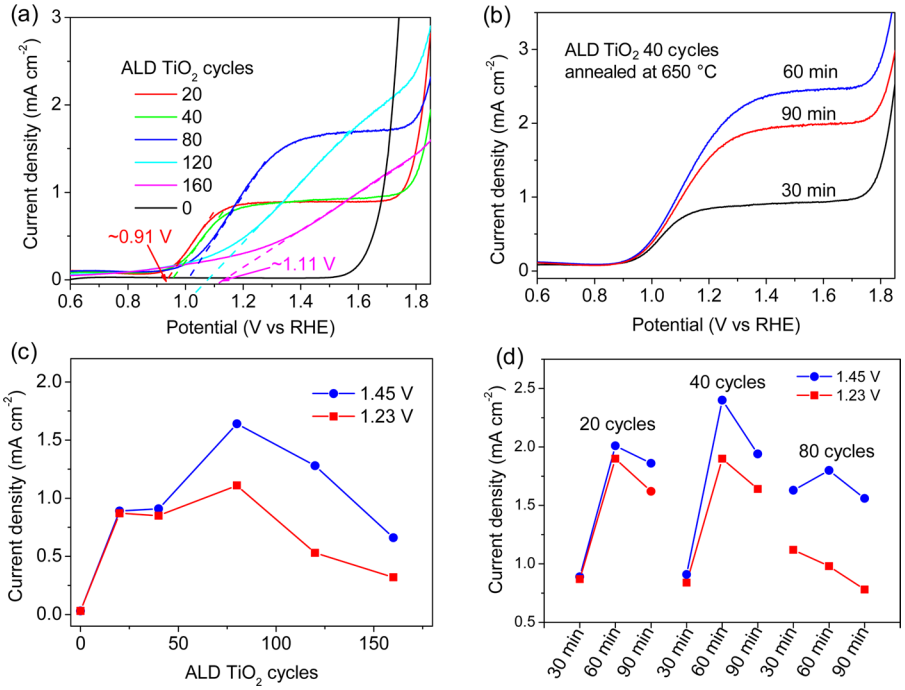

Figure 5. Photocurrent vs potential curves of hematite photoanodes with (a) different ALD TiO_2 cycles (650 °C annealing time: 30 min fixed), and (b) different annealing time at 650 °C (ALD TiO_2 40 cycles fixed). (c, d) Current densities for hematite photanodes with different ALD TiO_2 cycles and annealing time at 650 °C, respectively.

DOI: 10.1021/acsami.5b01394
ACS Appl. Mater. Interfaces 2015, 7, 16960–16966

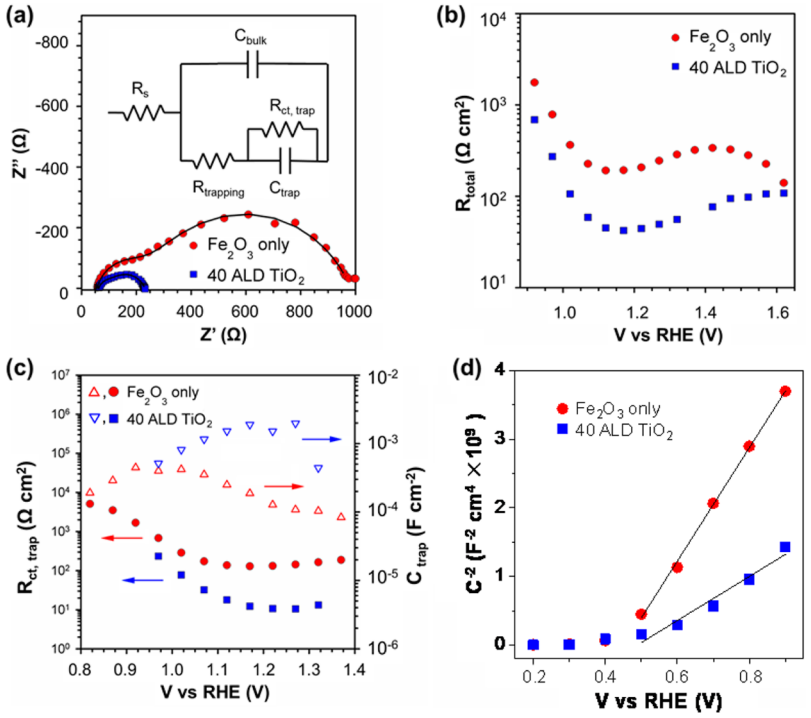

Figure 6. (a) Nyquist plots obtained at 1.15 V Vs RHE under illumination for the pristine F_2O_3 and the 40 ALD cycle TiO_2-coated F_2O_3 with 650 °C annealing samples. The lines represent the fitting employing the equivalent circuit in the inset. (b) Total charge transfer resistance ($R_{trapping}$ + $R_{ct,\ trap}$) and (c) C_{trap} and $R_{ct,\ trap}$, for both analyzed samples under illumination. (d) Mott−Schottky analysis obtained from C_{bulk} under dark conditions.

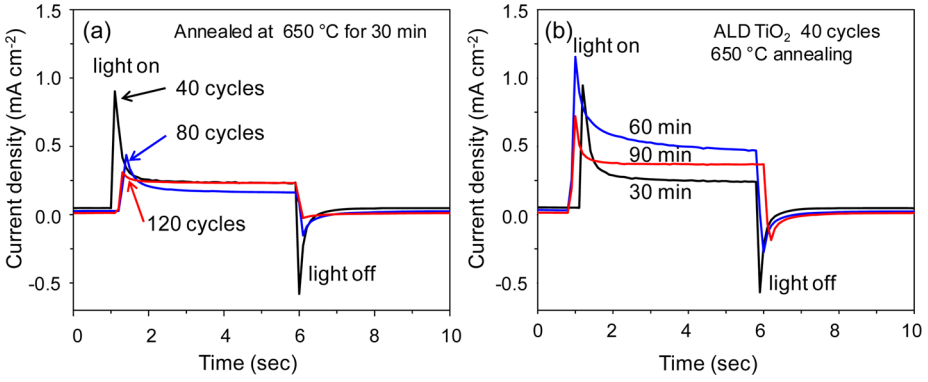

Figure 7. Transient photocurrent of the hematite nanorods arrays samples with (a) different ALD TiO_2 cycles and (b) different annealing time at 650 °C, potential 1.0 V vs RHE, 1 M NaOH.

voltage sweep across the working region. Representative Nyquist plots are shown in Figure 6a, featuring two semicircles in the impedance spectrum. The measured spectra were fitted to the equivalent circuit in the inset of Figure 6a comprising a series resistance (R_s), a bulk capacitance corresponding the Fe_2O_3 (C_{bulk}), a trapping resistance accounting for the charge transfer from the bulk to the traps ($R_{trapping}$), the capacitance of the traps (C_{trap}) and the charge transfer from the traps to the electrolyte ($R_{ct,\ trap}$). The valley of $R_{ct,\ trap}$ at a similar potential than the peak of C_{trap} (Figure 6c) confirms the presence of a surface states mediated charge transfer, following a previously reported trend with Fe_2O_3 systems.[32] In such a charge transfer process, the water oxidation takes place predominantly from surface trapped holes rather than from valence band holes. After being annealed at 650 °C, the ALD TiO_2 layer changes the distribution of the surface states, reflected on the C_{trap}, which reduces both $R_{trapping}$ and $R_{ct,\ trap}$. This results in a better total charge transfer resistance (Figure 6b) and enhances the performance. Figure 6d shows the Mott−Schottky plots of the pristine Fe_2O_3 and the 40 ALD cycles TiO_2 treated sample. The slopes determined from the Mott−Schottky plots are used to estimate the carrier densities using the equation; $N_D = (2/\epsilon_0\epsilon\varepsilon_0)[d(1/C^2)/dV]^{-1}$, where ϵ_0 is the electron charge (1.602×10^{-19} C), ε is the dielectric constant of α-Fe_2O_3 (80), ε_0 is the permittivity of vacuum (8.854×10^{-14} Fm^{-1}), N_D is the donor density, and V is the potential applied at the electrode.[30] The as-calculated carrier densities for pristine Fe_2O_3 and the 40 ALD cycle TiO_2-treated sample are similar, 2.13×10^{18} and 5.49×10^{18} cm^{-3}, respectively. The estimated flat band potential of the pristine Fe_2O_3 is around 0.45 V vs RHE, which is in line with previous reported values for nanostructured hematite.[24] No obvious flat band potential shift is observed for the ALD TiO_2-treated sample. The similar carrier density and flat band potential indicate that the Ti doping effect in this

DOI: 10.1021/acsami.5b01394
ACS Appl. Mater. Interfaces 2015, 7, 16960−16966

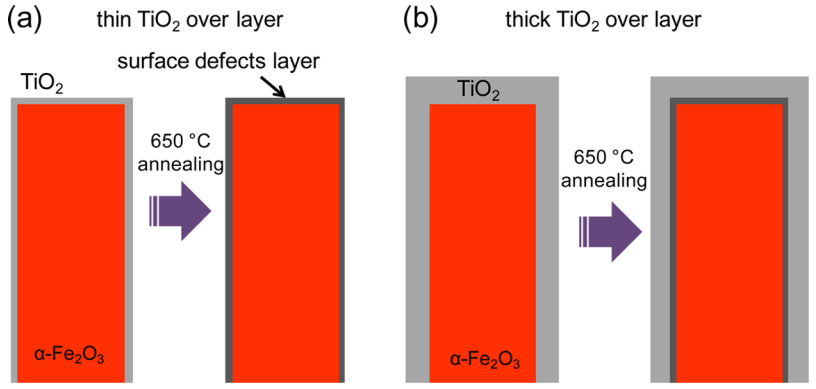

Figure 8. Schematics showing ALD TiO_2 overlayer thickness effect under 650 °C annealing, (a) with thin ALD over layers and (b) with thick ALD TiO_2 over layers.

study is insignificant. The dominant reason for the increase in photocurrent is the improved charge transfer on the hematite surface via the increased surface states after the ALD TiO_2 treatment.

To further investigate the ALD TiO_2 thickness and annealing time effect, we recorded transient photocurrents of the hematite samples under key bias, as these measurements have been reported to substantiate the effect of electron−hole recombination at the hematite surface in previous studies.[26,41] The transient photocurrent at 1.0 V vs RHE of hematite photoanodes with different ALD TiO_2 cycles and different annealing time at 650 °C are shown in Figure 7a, b, respectively. When light is turned on, photogenerated holes travel to the semiconductor−liquid junction (SCLJ) and accumulate because of the slow OER kinetics,[29] or because of trap states in the bulk and on the surface.[26−29,42] This induces a sharp anodic current spike, which decays until equilibrium is eventually reached between water oxidation and charge recombination. Conversely, the cathodic transient peak observed when the light is turned off has been assigned to electrons diffusing from the external circuit and recombining with the accumulated holes at the SCLJ. The transient photocurrent spike decreases when the ALD TiO_2 layer thickness increases at annealing conditions fixed at 650 °C for 30 min (Figure 7a). The smaller transient photocurrent spike means less hole accumulation at the SCLJ. When the ALD TiO_2 is 40 cycles and the annealing time at 650 °C is increased from 30 to 60 min, the photocurrent spike becomes much smaller (Figure 7b). When the annealing time is further increased to 90 min, the photocurrent spike looks similar to the 60 min one.

Our experiments lead us to conclude the effect of ALD TiO_2 overlayer thickness to the PEC performance of hematite photoanodes annealed at 650 °C, as shown in Figure 8. First, the Ti diffusion into the Fe_2O_3 increases the surface defect states, which enhances the trap-mediated charge transfer process at the hematite-electrolyte interface and hence improves the photocurrent. Because thermal diffusion is a concentration and time dependent process, the density of the defect states depends on both the TiO_2 thickness and the annealing time. This explains why the photocurrent increases with increasing annealing time (Figure 5b) at fixed ALD cycles. Second, if the TiO_2 layer is too thick, it will block the hole transfer. That could be the reason for the decreasing photocurrent for the thicker TiO_2 overlayer samples (Figure 5a), even it shows smaller transient photocurrent spike (Figure 7a). A moderate thickness of ALD TiO_2 over layer is therefore preferred because it can create sufficient defect states without blocking the hole transfer. Here, the optimized ALD TiO_2 thickness is about 2.4 nm with 40 ALD cycles annealed at 650 °C for 60 min.

4. CONCLUSIONS

In summary, an effective surface treatment by ALD of hematite nanorods for efficient water oxidation is reported. The increased PEC performance is mainly attributed to the enhanced hole transfer via surface trap at the hematite−electrolyte interface when an amorphous TiO_2 layer is observed. This enhanced PEC performance is observed when the ALD TiO_2 layer thickness is below a critical thickness. If the thickness is too thick, the hole transfer from hematite to liquid is blocked because of formation of a substantive heterojunction. A photocurrent of 1.9 mA cm^{-2} at 1.23 V (vs RHE) under AM 1.5 simulated solar illumination is achieved in optimized conditions.

■ ASSOCIATED CONTENT

Supporting Information

The Supporting Information is available free of charge on the ACS Publications website at DOI: 10.1021/acsami.5b01394.

SEM images, XRD, XPS, dark current curves, IPCE spectra, and $I-T$ curve (PDF)

■ AUTHOR INFORMATION

Corresponding Author

*E-mail: Lydiawong@ntu.edu.sg.

Notes

The authors declare no competing financial interest.

■ ACKNOWLEDGMENTS

Financial support from the Energy Innovation Research Programme Grant NRF2011EWT-CERP001-019 is kindly acknowledged. We thank Prof. Shen Ze Xiang for helping with the Raman study.

■ REFERENCES

(1) Fujishima, A.; Honda, K. Electrochemical Photolysis of Water at a Semiconductor Electrode. *Nature* **1972**, *238*, 37−38.

(2) Khaselev, O.; Turner, J. A. A Monolithic Photovoltaic-Photoelectrochemical Device for Hydrogen Production via Water Splitting. *Science* **1998**, *280*, 425−427.

DOI: 10.1021/acsami.5b01394
ACS Appl. Mater. Interfaces 2015, 7, 16960−16966

(3) Gratzel, M. Photoelectrochemical Cells. *Nature* **2001**, *414*, 338−344.
(4) Sivula, K.; Le Formal, F.; Grätzel, M. Solar Water Splitting: Progress Using Hematite (α-Fe_2O_3) Photoelectrodes. *ChemSusChem* **2011**, *4*, 432−449.
(5) Bassi, P. S.; Gurudayal; Wong, L. H.; Barber, J. Iron Based Photoanodes for Solar Fuel Production. *Phys. Chem. Chem. Phys.* **2014**, *16*, 11834−11842.
(6) Murphy, A. B.; Barnes, P. R. F.; Randeniya, L. K.; Plumb, I. C.; Grey, I. E.; Horne, M. D.; Glasscock, J. A. Efficiency of Solar Water Splitting using Semiconductor Electrodes. *Int. J. Hydrogen Energy* **2006**, *31*, 1999−2017.
(7) Sivula, K.; Zboril, R.; Le Formal, F.; Robert, R.; Weidenkaff, A.; Tucek, J.; Frydrych, J.; Grätzel, M. Photoelectrochemical Water Splitting with Mesoporous Hematite Prepared by a Solution-Based Colloidal Approach. *J. Am. Chem. Soc.* **2010**, *132*, 7436−7444.
(8) Xi, L.; Bassi, P. S.; Chiam, S. Y.; Mak, W. F.; Tran, P. D.; Barber, J.; Chye Loo, J. S.; Wong, L. H. Surface Treatment of Hematite Photoanodes with Ainc Acetate for Water Oxidation. *Nanoscale* **2012**, *4*, 4430−4433.
(9) Lin, Y.; Zhou, S.; Sheehan, S. W.; Wang, D. Nanonet-Based Hematite Heteronanostructures for Efficient Solar Water Splitting. *J. Am. Chem. Soc.* **2011**, *133*, 2398−2401.
(10) Li, X.; Fan, N. C.; Fan, H. J. A Micro-pulse Process of Atomic Layer Deposition of Iron Oxide Using Ferrocene and Ozone Precursors and Ti-Doping. *Chem. Vap. Deposition* **2013**, *19*, 104−110.
(11) Riha, S. C.; Klahr, B. M.; Tyo, E. C.; Seifert, S.; Vajda, S.; Pellin, M. J.; Hamann, T. W.; Martinson, A. B. F. Atomic Layer Deposition of a Submonolayer Catalyst for the Enhanced Photoelectrochemical Performance of Water Oxidation with Hematite. *ACS Nano* **2013**, *7*, 2396−2405.
(12) Tilley, S. D.; Cornuz, M.; Sivula, K.; Grätzel, M. Light-Induced Water Splitting with Hematite: Improved Nanostructure and Iridium Oxide Catalysis. *Angew. Chem., Int. Ed.* **2010**, *49*, 6405−6408.
(13) Vayssieres, L.; Beermann, N.; Lindquist, S.-E.; Hagfeldt, A. Controlled Aqueous Chemical Growth of Oriented Three-Dimensional Crystalline Nanorod Arrays: Application to Iron(III) Oxides. *Chem. Mater.* **2000**, *13*, 233−235.
(14) Xi, L.; Tran, P. D.; Chiam, S. Y.; Bassi, P. S.; Mak, W. F.; Mulmudi, H. K.; Batabyal, S. K.; Barber, J.; Loo, J. S. C.; Wong, L. H. Co_3O_4-Decorated Hematite Nanorods As an Effective Photoanode for Solar Water Oxidation. *J. Phys. Chem. C* **2012**, *116*, 13884−13889.
(15) Kim, J. Y.; Magesh, G.; Youn, D. H.; Jang, J.-W.; Kubota, J.; Domen, K.; Lee, J. S. Single-crystalline, Wormlike Hematite Photoanodes for Efficient Solar Water Splitting. *Sci. Rep.* **2013**, *3*, 2681.
(16) Beermann, N.; Vayssieres, L.; Lindquist, S. E.; Hagfeldt, A. Photoelectrochemical Studies of Oriented Nanorod Thin Films of Hematite. *J. Electrochem. Soc.* **2000**, *147*, 2456−2461.
(17) Mohapatra, S. K.; John, S. E.; Banerjee, S.; Misra, M. Water Photooxidation by Smooth and Ultrathin α-Fe_2O_3 Nanotube Arrays. *Chem. Mater.* **2009**, *21*, 3048−3055.
(18) Sivula, K.; Formal, F. L.; Grätzel, M. WO_3−Fe_2O_3 Photoanodes for Water Splitting: A Host Scaffold, Guest Absorber Approach. *Chem. Mater.* **2009**, *21*, 2862−2867.
(19) Lin, Y.; Yuan, G.; Sheehan, S.; Zhou, S.; Wang, D. Hematite-based Solar Water Splitting: Challenges and Opportunities. *Energy Environ. Sci.* **2011**, *4*, 4862−4869.
(20) Jorand Sartoretti, C.; Alexander, B. D.; Solarska, R.; Rutkowska, I. A.; Augustynski, J.; Cerny, R. Photoelectrochemical Oxidation of Water at Transparent Ferric Oxide Film Electrodes. *J. Phys. Chem. B* **2005**, *109*, 13685−13692.
(21) Jang, J. S.; Lee, J.; Ye, H.; Fan, F.-R. F.; Bard, A. J. Rapid Screening of Effective Dopants for Fe_2O_3 Photocatalysts with Scanning Electrochemical Microscopy and Investigation of Their Photoelectrochemical Properties. *J. Phys. Chem. C* **2009**, *113*, 6719−6724.
(22) Gurudayal; Chiam, S. Y.; Kumar, M. H.; Bassi, P. S.; Seng, H. L.; Barber, J.; Wong, L. H. Improving the Efficiency of Hematite Nanorods for Photoelectrochemical Water Splitting by Doping with Manganese. *ACS Appl. Mater. Interfaces* **2014**, *6*, 5852−5859.
(23) Kleiman-Shwarsctein, A.; Hu, Y.-S.; Forman, A. J.; Stucky, G. D.; McFarland, E. W. Electrodeposition of α-Fe_2O_3 Doped with Mo or Cr as Photoanodes for Photocatalytic Water Splitting. *J. Phys. Chem. C* **2008**, *112*, 15900−15907.
(24) Ling, Y.; Wang, G.; Wheeler, D. A.; Zhang, J. Z.; Li, Y. Sn-Doped Hematite Nanostructures for Photoelectrochemical Water Splitting. *Nano Lett.* **2011**, *11*, 2119−2125.
(25) Wang, G.; Ling, Y.; Wheeler, D. A.; George, K. E. N.; Horsley, K.; Heske, C.; Zhang, J. Z.; Li, Y. Facile Synthesis of Highly Photoactive α-Fe_2O_3-Based Films for Water Oxidation. *Nano Lett.* **2011**, *11*, 3503−3509.
(26) Le Formal, F.; Tetreault, N.; Cornuz, M.; Moehl, T.; Gratzel, M.; Sivula, K. Passivating Surface States on Water Splitting Hematite Photoanodes with Alumina Overlayers. *Chem. Sci.* **2011**, *2*, 737−743.
(27) Iwanski, P.; Curran, J. S.; Gissler, W.; Memming, R. The Photoelectrochemical Behavior of Ferric Oxide in the Presence of Redox Reagents. *J. Electrochem. Soc.* **1981**, *128*, 2128−2133.
(28) Dare-Edwards, M. P.; Goodenough, J. B.; Hamnett, A.; Trevellick, P. R. Electrochemistry and photoelectrochemistry of iron(III) oxide. *J. Chem. Soc., Faraday Trans. 1* **1983**, *79*, 2027−2041.
(29) Sanchez, C.; Sieber, K. D.; Somorjai, G. A. The Photoelectrochemistry of Niobium doped α-Fe_2O_3. *J. Electroanal. Chem. Interfacial Electrochem.* **1988**, *252*, 269−290.
(30) Xi, L.; Chiam, S. Y.; Mak, W. F.; Tran, P. D.; Barber, J.; Loo, S. C. J.; Wong, L. H. A Novel Strategy for Surface Treatment on Hematite Photoanode for Efficient Water Oxidation. *Chem. Sci.* **2013**, *4*, 164−169.
(31) Yang, X.; Liu, R.; Du, C.; Dai, P.; Zheng, Z.; Wang, D. Improving Hematite-based Photoelectrochemical Water Splitting with Ultrathin TiO_2 by Atomic Layer Deposition. *ACS Appl. Mater. Interfaces* **2014**, *6*, 12005−12011.
(32) Klahr, B.; Gimenez, S.; Fabregat-Santiago, F.; Hamann, T.; Bisquert, J. Water Oxidation at Hematite Photoelectrodes: The Role of Surface States. *J. Am. Chem. Soc.* **2012**, *134*, 4294−4302.
(33) Paracchino, A.; Mathews, N.; Hisatomi, T.; Stefik, M.; Tilley, S. D.; Gratzel, M. Ultrathin Films on Copper(i) Oxide Water Splitting Photocathodes: a Study on Performance and Stability. *Energy Environ. Sci.* **2012**, *5*, 8673−8681.
(34) de Faria, D. L. A.; Venâncio Silva, S.; de Oliveira, M. T. Raman Microspectroscopy of Some Iron Oxides and Oxyhydroxides. *J. Raman Spectrosc.* **1997**, *28*, 873−878.
(35) Li, Q.; Liu, B.; Li, Y.; Liu, R.; Li, X.; Li, D.; Yu, S.; Liu, D.; Wang, P.; Li, B.; Zou, B.; Cui, T.; Zou, G. Ethylene Glycol-mediated Synthesis of Nanoporous Anatase TiO_2 Rods and Rutile TiO_2 Self-assembly Chrysanthemums. *J. Alloys Compd.* **2009**, *471*, 477−480.
(36) Onari, S.; Arai, T.; Kudo, K. Infrared Lattice Vibrations and Dielectric Dispersion in Span Class. *Phys. Rev. B* **1977**, *16*, 1717−1721.
(37) Bersani, D.; Lottici, P. P.; Montenero, A. Micro-Raman Investigation of Iron Oxide Films and Powders Produced by Sol−gel Syntheses. *J. Raman Spectrosc.* **1999**, *30*, 355−360.
(38) Zoppi, A.; Lofrumento, C.; Castellucci, E. M.; Sciau, P. Al-for-Fe Substitution in Hematite: the Effect of Low Al Concentrations in the Raman Spectrum of Fe_2O_3. *J. Raman Spectrosc.* **2008**, *39*, 40−46.
(39) Chen, X.; Liu, L.; Yu, P. Y.; Mao, S. S. Increasing Solar Absorption for Photocatalysis with Black Hydrogenated Titanium Dioxide Nanocrystals. *Science* **2011**, *331*, 746−750.
(40) Wang, L.; Lee, C.-Y.; Schmuki, P. Ti and Sn Co-doped Anodic α-Fe_2O_3 Films for Efficient Water Splitting. *Electrochem. Commun.* **2013**, *30*, 21−25.
(41) Cao, D.; Luo, W.; Feng, J.; Zhao, X.; Li, Z.; Zou, Z. Cathodic Shift of Onset Potential for Water Oxidation on a Ti^{4+} Doped Fe_2O_3 Photoanode by Suppressing the Back Reaction. *Energy Environ. Sci.* **2014**, *7*, 752−759.
(42) Le Formal, F.; Grätzel, M.; Sivula, K. Controlling Photoactivity in Ultrathin Hematite Films for Solar Water-Splitting. *Adv. Funct. Mater.* **2010**, *20*, 1099−1107.

DOI: 10.1021/acsami.5b01394
ACS Appl. Mater. Interfaces 2015, 7, 16960−16966